References

[1] Jaffe, N. A., Clark, K. J., Nardo, C. T., and Anderson, L. W., "Nosetip Cooling Technology Program," Final Report 73-84, Air Force Contract F04701-71-C-0087, Oct. 1973, Aerotherm Div., Acurex Corp., Mountain View, Calif.

[2] Clark, K. J. and Mehner, P. O., "Test Report, Nosetip Cooling Technology Program, Combined Cooling Tests," Air Force Contract F04701-71-C-0087, Sept. 30, 1974.

[3] Lane, F., "Liquid-Layer Phenomenology," KLD TR-6, Feb. 1972, KLD Associates, Huntington, New York.

[4] Baronti, P., Fox, H., and Soll, D., "A Survey of the Compressible Turbulent Boundary Layer with Mass Transfer," *Astronautic Data*, Vol 13, 1967, pp. 239–249.

[5] Covington, M. A. and Vojvodich, N. S., "Turbulent Flow Studies in Two Arc-Heated Duct Facilities," *Journal of Spacecraft and Rockets*, Vol. 9, No. 6, June 1972, pp. 441–447.

[6] Jorgensen, L. H. and Baum, G. M., "Charts for Equilibrium Flow Properties of Air in Hypervelocity Nozzles," TND-1333, 1962, NASA.

[7] Moeckel, W. E. and Weston, K. C., "Composition and Thermodynamic Properties of Air in Chemical Equilibrium," TN-4265, 1958, NACA.

[8] Charwat, A. F., "Supersonic Flows with Imbedded Separated Regions," *Advances in Heat Transfer*, Vol. 6, Academic Press, New York, 1970, pp. 1–132.

[9] Schlichting, H., *Boundary Layer Theory*, 4th ed., McGraw-Hill, New York, 1960.

[10] Nardo, C. T., "Discrete Injection Blockage Condition," Aerotherm Div., Acurex Corp., Mountain View, Calif., to be published.

DECEMBER 1974 AIAA JOURNAL VOL. 12, NO. 12

Mathematical Modeling for the Detection of Fish by an Airborne Laser

DAVID L. MURPHREE,* CLAYBORNE D. TAYLOR,† AND RONALD W. MCCLENDON‡

Mississippi State University, Mississippi State, Miss.

To assess the feasibility of an airborne remote sensing laser system for fish detection, a mathematical model was developed and solved which incorporated the physical interactions involved in the process of laser transmission through the air/sea interface and ocean environment. For a circular laser beam incident normal to the ocean surface, the power density was determined beneath the ocean surface as a function of surface roughness (wind velocity) and depth. Using the principle of electromagnetic reciprocity, the power reflected from submerged targets and detected at the airborne receiver was determined. The results from the developed mathematical model, using input parameters of presently available equipment and estimates of fish school density and reflectivity, reveal that the power received at an airborne detector from fish reflected incident laser radiation and the signal-to-noise ratio (S/N) are of sufficient magnitude to locate fish schools with an airborne remote sensing laser system.

I. Introduction

THE recent advances in high-powered lasers operating in the blue-green part of the optical spectrum have led to the possibility of the development of an airborne remote sensing laser system for detection and quantification of objects submerged beneath the ocean surface. The incident laser radiation would be reflected from the submerged objects and detected at an airborne receiver. Such a system would enable location, identification, quantification, and assessment of fish resources.

An aircraft cruising at 160 km/hr while illuminating a 75-m width transverse to the flight direction would search 12 sq km of ocean surface per hour. A 500 pulse/sec laser, illuminating a circular area on the ocean surface of 1 m in diameter per pulse, would thoroughly cover the 75-m width by employing 31 pulses while sweeping the laser beam transverse to the plane's flight direction. The maximum beam angle with respect to the vertical would be 13.8° for a 500-ft altitude. It is necessary to maintain the laser beam diameter on the ocean surface no larger than approximately 1 m in order to maintain a high-power density. The distance between the center of each surface circular illuminated area would be 2.5 m in the transverse direction and 2.7 m in the direction of flight. Underwater beam spreading due to refraction by the distribution of surface facets would insure complete coverage of the underwater regions under investigation.

Received December 26, 1973; revision received June 24, 1974. This research was supported by the National Marine Fisheries Service, Bay St. Louis Fisheries Engineering Laboratory under Contract 03-3-042-27.

Index categories: Lasers; Oceanography, Physical and Biological; Atmospheric, Space, and Oceanographic Sciences.

* Professor of Aerospace Engineering.

† Professor of Electrical Engineering.

‡ Graduate Student, Department of Aerophysics and Aerospace Engineering.

II. Analysis

In order to determine the power density distribution beneath the ocean surface when it is illuminated by a collimated beam of monochromatic light, certain convenient considerations are made. In general, the development followed for the underwater power density is that presented by Swennen.[1]

The ocean surface is considered to be described in terms of a probability distribution of local slopes. Using a Gaussian distribution modified by a Gram-Charlier series to include the effects of wind direction and velocity, Cox and Munk[2] obtained the following empirical relationship for the statistical distribution of slopes on the ocean surface:

$$p(\alpha,\beta)=\frac{e^{-(\xi^2+\eta^2)/2}}{2\pi\sigma_c\sigma_u}\left[1-\tfrac{1}{2}C_{21}(\xi^2-1)\eta-\tfrac{1}{6}C_{03}(\eta^3-3\eta)+\tfrac{1}{24}C_{40}(\xi^4-6\xi^2+3)+\tfrac{1}{4}C_{22}(\xi^2-1)(\eta^2-1)+\tfrac{1}{24}C_{04}(\eta^4-6\eta^2+3)\right] \quad (1)$$

where

$$\xi=\frac{\tan\beta\sin(\alpha-\Psi)}{\sigma_c} \quad (2a)$$

$$\eta=\frac{\tan\beta\cos(\alpha-\Psi)}{\sigma_u} \quad (2b)$$

$$\sigma_c^2=0.003+0.00192W \quad (2c)$$

$$\sigma_u^2=0.00316W \quad (2d)$$

$$C_{21} = 0.01 - 0.0086W \tag{2e}$$
$$C_{03} = 0.04 - 0.033W \tag{2f}$$
$$C_{40} = 0.40 \tag{2g}$$
$$C_{22} = 0.12 \tag{2h}$$
$$C_{04} = 0.23 \tag{2i}$$

with β the angle formed by the line of steepest ascent of the elementary facet and its projection onto the horizontal plane, α the angle formed by the foregoing projection and the plane of incidence ($\alpha = 0$ is directed toward the laser source), θ_0 the angle between the incident laser ray and the z axis, Ψ the angle between the wind direction and the plane of incidence with the y' axis pointing towards the "wind-source," and W the wind velocity in m/sec. Figure 1 presents the geometry of a surface facet and a refracted incident laser ray. The angle μ is formed by a ray refracted to the point of observation by the surface facet under consideration and the z axis, and the angle v is formed by the projection of this refracted ray onto the horizontal plane and the y axis. Because of limitations inherent in the method used for obtaining this distribution function, its range of applicability is limited by the following restrictions:

$$|\xi| \leqq 2.5 \tag{3a}$$
$$|\eta| \leqq 2.5 \tag{3b}$$
$$W \leqq 14 \text{ m/sec} \tag{3c}$$

The incident beam is considered to be cylindrical with a uniform power density P_0 incident on the ocean surface at an angle θ_0 with the normal. The radius of the beam circular cross section is designated as a.

The surface transmittance depends not only on the angle of incidence but also on the incident polarization. Since there is a distribution of surface facets there is hence a distribution of incident polarizations. The surface transmittance is thus approximated by the average of the transmittances for parallel and perpendicular incident polarizations

$$\tau = (\tau_{\parallel} + \tau_{\perp})/2 \tag{4}$$

where $\tau_{\parallel}$ is the transmittance for the incident electric field parallel to the plane of incidence, and $\tau_{\perp}$ is the transmittance for the incident electric field perpendicular to the plane of incidence. For the angle of incidence ω_i and angle of refraction ω_r the surface transmittance is[3]

$$\tau = \frac{1}{2}\frac{\sin 2\omega_i \sin 2\omega_r}{\sin^2(\omega_i+\omega_r)}\frac{1+\cos^2(\omega_i-\omega_r)}{\cos^2(\omega_i-\omega_r)} \tag{5}$$

In the limit of normal incidence the foregoing becomes

$$\tau = 4n/(n+1)^2 \tag{6}$$

where n is the index of refraction of sea water, $n = 1.33$.

As the laser radiation propagates through sea water it is both absorbed and scattered. The power density $P(r)$ at a distance r in a collimated light beam of power density P_0 at $r = 0$ is

$$P(r) = P_0 e^{-\gamma r} \tag{7}$$

where γ is the volume attenuation coefficient equal to the sum of the volume absorption coefficient and the total volume scattering coefficient.

Since there is a distribution of continually varying surface facets, one may neglect the phase differences that occur and simply add the power contributions for elementary surface facets. The total power density at the underwater point of observation is thus obtained by adding the contributions from all refracting elementary facets contained within the beam cross section. Therefore, integrating over the beam illuminated facets yields the power density at a point (μ_0, v_0, z) beneath the surface due to normally incident laser radiation on the surface

$$P_d(\mu_0, v_0, z) = \int_{-\pi}^{\pi} d\alpha \int_0^{\pi/2} d\beta\, \tau P_0 \exp(-\gamma|z|\sec\mu)\cdot \cos\omega_i \sec\omega_r \cos\lambda\, p(\alpha,\beta)\tan\beta\sec^2\beta f(\mu, v) \tag{8}$$

where

$$\cos\lambda = \cos\mu\cos\mu_0 + \sin\mu\sin\mu_0\cos(v - v_0) \tag{9a}$$

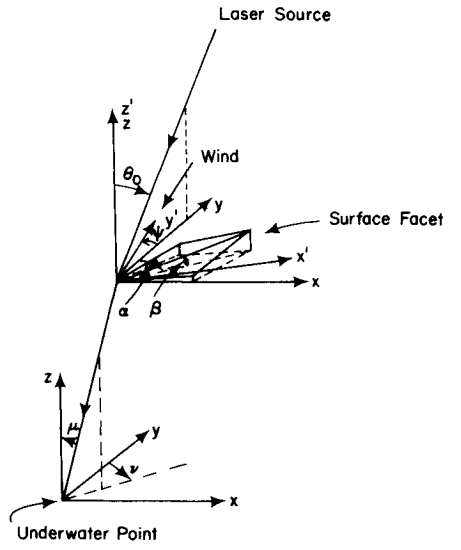

Fig. 1 Coordinate systems for a surface facet and the underwater points of interest.

$$\cos\omega_i = \cos\theta_0\cos\beta - \sin\theta_0\cos\alpha\sin\beta \tag{9b}$$
$$\cos\omega_r = (\cos^2\omega_i + n^2 - 1)^{1/2}/n \tag{9c}$$
$$\cos\mu = (\cos\theta_0 + k\cos\beta)/n \tag{9d}$$
$$\cot v = \cot\alpha - \sin\theta_0/(k\sin\alpha\sin\beta) \tag{9e}$$
$$k = (\sin\theta_0\cos\alpha\sin\beta - \cos\theta_0\cos\beta) + [(\sin\theta_0\cos\alpha\sin\beta - \cos\theta_0\cos\beta)^2 + n^2 - 1]^{1/2} \tag{9f}$$
$$f(\mu, v) = \begin{cases} 1 & \mu_{\min} \leqq \mu \leqq \mu_{\max},\ v_{\min} \leqq v \leqq v_{\max} \\ 0 & \text{otherwise} \end{cases} \tag{9g}$$
$$v_{\min} = \begin{cases} -\pi & |z|\tan\mu_0 \leqq a \\ v_0 - \sin^{-1}(a/|z|\tan\mu_0) & |z|\tan\mu_0 > a \end{cases} \tag{9h}$$
$$v_{\max} = \begin{cases} \pi & |z|\tan\mu_0 \leqq a \\ v_0 + \sin^{-1}(a/|z|\tan\mu_0) & |z|\tan\mu_0 > a \end{cases} \tag{9i}$$
$$\mu_{\min} = \begin{cases} 0 & |z|\tan\mu_0 \leqq a \\ \tan^{-1}(x^-/|z|) & |z|\tan\mu_0 > a \end{cases} \tag{9j}$$
$$\mu_{\max} = \tan^{-1}(x^+/|z|) \tag{9k}$$
$$x^{\pm} = |z|\tan\mu_0\cos(v - v_0) \pm [a^2 - (|z|\tan\mu_0)^2\sin^2(v - v_0)]^{1/2} \tag{9l}$$

The coordinates (μ_0, v_0, z) locate the point at which the power density is calculated underneath the water surface. The depth of the point beneath the water surface is given by z and the angles μ_0 and v_0 are referenced to the center of the laser beam circular cross section on the water surface, as indicated in Fig. 2.

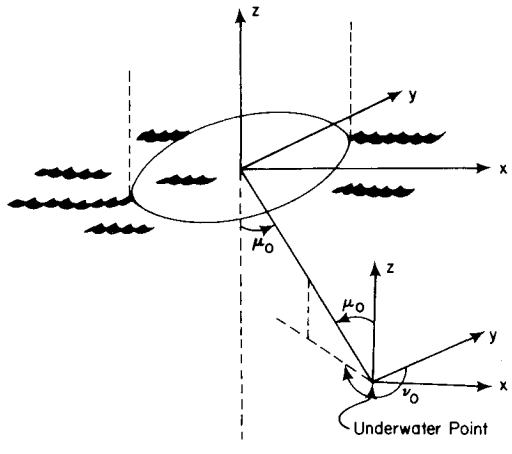

Fig. 2 Underwater point at which power density is calculated referenced to the center of laser beam on water surface.

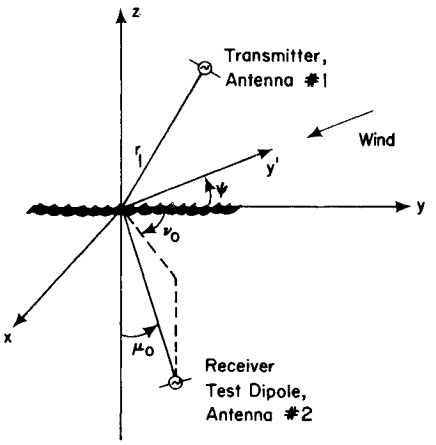

Fig. 3 Airborne transmitting antenna and underwater receiving antenna.

Equations (8) and (9) are for normal incidence of the laser radiation on the ocean surface. The values for $\mu_{\min}$ and $\mu_{\max}$ used differ in form from those given by Swennen.[1] The form of $\mu_{\min}$ and $\mu_{\max}$ derived by Swennen required double precision in the computer analysis to obtain the desired accuracy, while the forms employed in the present analysis give sufficient accuracy employing single precision.

To determine the power reflected from the underwater targets back through the ocean surface, electromagnetic reciprocity is used.[4] The form of the electromagnetic reciprocity principle applying to antennas is: If an arbitrarily located antenna (called antenna 1) is driven by voltage V and thereby produces a short circuit current I in an arbitrarily located receiving antenna (called antenna 2), then using antenna 2 for transmitting by driving it with voltage V and using antenna 1 for reception results in short circuit current I being induced in antenna 1 by antenna 2. The configuration considered is shown in Fig. 3. Antenna 1 is the antenna above the water located at the position of the airborne laser and detector, and antenna 2 is located at the position of the underwater target.

The electric field produced by antenna 1 at a distance $\mathbf{r}_1$ from the antenna, $\mathbf{E}^{\text{rad}}_{1(\mathbf{r}_1)}$, may be expressed as[4]

$$\mathbf{E}^{\text{rad}}_{1(\mathbf{r}_1)} = j\frac{\zeta_0 I_1{}^{\text{rad}}}{2\lambda r_1}\exp(-j\mathbf{k}\cdot\mathbf{r}_1)\,\mathbf{h}_1(\mu, v) \tag{10}$$

where λ is the radiated wavelength, $I_1{}^{\text{rad}}$ is the antenna current, $\zeta_0 = (\mu_0'/\varepsilon_0')^{1/2}$ is the intrinsic wave impedance of the ambient medium, μ_0' and ε_0' are the permeability and permittivity of the medium, respectively, j is $(-1)^{1/2}$, $\mathbf{k}$ is the vector wave number $\hat{k}k$ with $k = 2\pi/\lambda$, and $\mathbf{h}_1(\mu, v)$ is the complex effective vector length for antenna 1. Considering $\mathbf{r}_1$ to be the path length of the radiated beam from the source to the ocean surface, the incident power density at the ocean surface is

$$P_0 = \frac{1}{2\zeta_0}|\mathbf{E}_1{}^{\text{rad}}\cdot\hat{k}|^2 = \frac{\zeta_0|I_1{}^{\text{rad}}|^2}{8\lambda^2}\frac{|\mathbf{h}_1(\pi-\theta_0,\pi)\cdot\hat{k}|^2}{r_1{}^2} \tag{11}$$

The electric field produced by antenna 1 at antenna 2 in terms of the incident power density $P_d(\mu_0, v_0, z)$ of Eq. (8) is

$$\begin{aligned}|E_2| &= (2\zeta P_d)^{1/2}\\ &= (2\zeta_0 P_d/n)^{1/2}\end{aligned} \tag{12}$$

where

$$\zeta = (\mu'/\varepsilon')^{1/2} \tag{13}$$

is the intrinsic wave impedance of the water and

$$\zeta_0 = \zeta/(\varepsilon_0'/\varepsilon')^{1/2} = n\zeta \tag{14}$$

since the index of refraction n is

$$n = (\mu'\varepsilon')^{1/2}/(\mu_0'\varepsilon_0')^{1/2} \tag{15}$$

and

$$\mu_0' \approx \mu' \tag{16}$$

The open circuit voltage at antenna 2 is

$$V_2{}^{oc} = h_2 E_2/(2)^{1/2} \tag{17}$$

where h_2 is the complex effective vector length for antenna 2. A factor of $1/(2)^{1/2}$ is introduced to account for the distribution of polarizations incident on antenna 2.

A mutual impedance between antennas 1 and 2, Z_{12}, may be obtained

$$Z_{12} = V_2{}^{oc}/I_1{}^{\text{rad}} \tag{18}$$

and from the foregoing

$$|Z_{12}| = \frac{\zeta_0|h_1 h_2|}{2\lambda r_1}\left(\frac{P_d}{2nP_0}\right)^{1/2} \tag{19}$$

If the test dipole (antenna 2) is now used for transmission and antenna 1 is used for the reception, then according to the reciprocity theorem applied to antennas

$$|V_1{}^{oc}| = |Z_{12}|\,|I_2{}^{\text{rad}}| \tag{20}$$

The power density at antenna 1 is now

$$P_1 = \frac{1}{2\zeta_0}|E_1|^2 \tag{21}$$

where E_1 is the electric field produced at antenna 1 by antenna 2. However,

$$\begin{aligned}|E_1| &= \frac{(2)^{1/2}|V_1{}^{oc}|}{|h_1|}\\ &= \frac{\zeta_0|h_2|}{2\lambda r_1}\left(\frac{P_d}{nP_0}\right)^{1/2}|I_2{}^{\text{rad}}|\end{aligned} \tag{22}$$

and therefore

$$P_1 = \frac{\zeta_0}{8\lambda^2 r_1{}^2}\frac{P_d}{nP_0}|h_2|^2\,|I_2{}^{\text{rad}}|^2 \tag{23}$$

We may define an equivalent target surface area, A_t, from which the underwater target reflects the incident power density. Also we define an average surface reflectance R_t for the target. Then the power reflected from the target located at (μ_0, v_0, z) is

$$P^{\text{ref}}_{(\mu_0, v_0, z)} = R_t A_t P_d(\mu_0, v_0, z) \tag{24}$$

Considering the energy reflected back toward the air-sea interface from the target located at (μ_0, v_0, z) to be distributed isotropically into 2π steradians, then the power density of the reflected radiation above the underwater target, $P^{\text{ref}}(\mathbf{r})$, is

$$P^{\text{ref}}(\mathbf{r}) = R_t A_t P_d/2\pi r^2 \tag{25}$$

where $\mathbf{r}$ is the distance from the target to the point in question. Also

$$\begin{aligned}P^{\text{ref}}(\mathbf{r}) &= \frac{1}{2\zeta}|E_2{}^{\text{rad}}|^2\\ &= \frac{\zeta|I_2{}^{\text{rad}}|^2}{8\lambda^2}\frac{|h_2|^2}{r^2}\end{aligned} \tag{26}$$

Therefore

$$|I_2{}^{\text{rad}}|^2\,|h_2|^2 = \frac{4\lambda^2 R_t A_t P_d}{\pi\zeta} \tag{27}$$

and, from Eq. (23), the power density at antenna 2 becomes

$$P_1 = \frac{R_t A_t}{2\pi r_1{}^2}\left[\frac{P_d}{P_0}\right]^2 P_0 \tag{28}$$

Two inherent assumptions are made in applying the reciprocity theorem to obtain the power return from an underwater target. It is assumed that the power is scattered from the underwater target in the power pattern of a dipole antenna in the region above the target with no power scattered in the region below the target. The axis of the dipole is perpendicular to the direction of incidence. It is also assumed that the power is received by the receiver above the water with the same directivity as the transmitter system. In other words, only those scattered rays that egress through the illuminated spot on the ocean surface are considered to contribute to the received power.

The power received by a receiver above the ocean surface is

$$P^{\text{rec}} = P_1 A_r \tag{29}$$

where A_r is the effective antenna receiving cross section. It is more convenient to express Eq. (28) in terms of the power output of the radiator (laser) above the ocean surface. Since

$$P_0 = p^{\text{rad}}/(\pi a^2) \tag{30}$$

where p^{rad} is the radiated power, then

$$P_1 = \frac{R_t A_t}{2\pi^2 r_1^2 a^2}\left[\frac{P_d}{P_0}\right]^2 p^{\text{rad}} \tag{31}$$

and

$$p^{\text{rec}}_{(\mu_0, \nu_0, z)} = \frac{R_t A_t A_r}{2\pi^2 r_1^2 a^2}\left[\frac{P_d(\mu_0, \nu_0, z)}{P_0}\right]^2 p^{\text{rad}} \tag{32}$$

Equation (32) is the power received at the airborne detector from an underwater target located at (μ_0, ν_0, z) where the power density of the incident laser radiation is given by Eq. (8). A summation must be performed over all underwater points (μ_0, ν_0, z) to obtain the total power received at the airborne detector. To obtain this summation the underwater target area for a constant z is divided into a series of successive concentric circles, beginning with a circle of radius R_1. The center of each circle is located directly below the center of the laser illuminated circular region on the ocean surface. The radius of each successive circle is given by

$$R_n = nR_1, \qquad n = 1, 2, 3, \ldots \tag{33}$$

The concentric circles form a series of annuli, the area of each annulus given by

$$\text{annulus area} = \pi(R_{n+1}^2 - R_n^2) \tag{34}$$

The ratio of the annulus area between two successive circles of radius R_n and R_{n+1} to the area of the inner circle of radius R_1 is

$$\text{ratio} = \frac{\pi(R_{n+1}^2 - R_n^2)}{\pi R_1^2} \tag{35}$$

or

$$\text{ratio} = \frac{\pi[(n+1)^2 R_1^2 - n^2 R_1^2]}{\pi R_1^2} = 2n+1 \tag{36}$$

The area of the nth annulus is therefore

$$A_n = (2n+1)A_0 \tag{37}$$

where

$$A_0 = \pi R_1^2 \tag{38}$$

The underwater surface area of constant z can therefore be described in a grid pattern as shown in Fig. 4, where each grid element is of equal area ΔA, equal to the area of the inner circle, A_0.

The power received at the airborne detector from targets within a grid element located at (μ_0, ν_0, z) is given by Eq. (32) in the form

$$p^{\text{rec}}_{(\mu_0, \nu_0, z)} = \frac{R_t \varepsilon \Delta A A_r}{2\pi^2 r_1^2 a^2}\left[\frac{P_d(\mu_0, \nu_0, z)}{P_0}\right]^2 p^{\text{rad}} \tag{39}$$

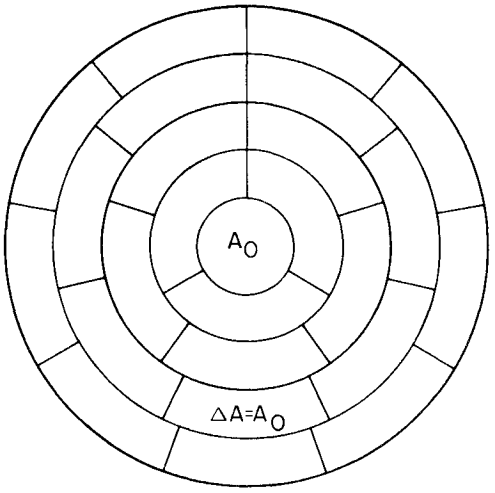

Fig. 4 Underwater target grid pattern.

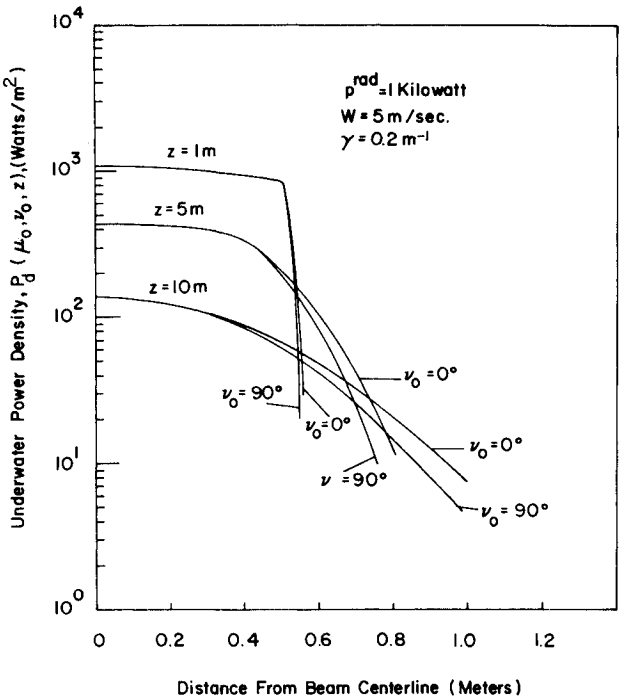

Fig. 5 Underwater power density distribution.

where ε is the ratio of the equivalent target surface area in the grid element of area ΔA located at (μ_0, ν_0, z), from which the underwater targets reflect the incident laser radiation, to the grid element area ΔA, i.e.,

$$A_t = \varepsilon \Delta A \tag{40}$$

The underwater power density $P_d(\mu_0, \nu_0, z)$ for each element $\Delta A(\mu_0, \nu_0, z)$ is determined at the centroid of the element at a radius r_n from the center of the inner circle, i.e.,

$$r_n = \left(\frac{R_{n+1}^2 + R_n^2}{2}\right)^{1/2} \qquad n = 1, 2, 3, \ldots \tag{41}$$

with

$$r_0 = R_1/(2)^{1/2} \tag{42}$$

Summing Eq. (39) over all grid elements which contribute to the total received power gives the total power detected by the airborne receiver scattered off the underwater targets. The criterion employed to determine the "cut-off" for the summation was to cease the summation at the outer annulus from which the power detected from that annulus was below the noise level of the detector.

III. Results

The power density at a point (μ_0, ν_0, z) beneath the ocean surface is calculated with Eq. (8) and the power received at the airborne detector from targets within a grid element located at (μ_0, ν_0, z) is calculated with Eq. (39). The total power received from target reflection is obtained by summing over all targets, or grid elements, which contribute to the total received power. The "cut-off" employed was 10^{-8} w (10% of the minimum detectable power of an RCA C21117C 40 mm SIT camera tube, but approximately the minimum detectable power of some photodiodes). Only laser radiation incident normal to the ocean surface was considered in the present analysis. For normal incidence, the y' and y axes of Fig. 1 can be considered to coincide; i.e., $\Psi = 0$.

Table 1 presents the input data employed for the calculations of Figs. 5–10. The system parameters, such as laser power and receiver area, were based on presently available equipment suitable for incorporation in an airborne remote sensing laser system for fish detection. The ratio of target area to grid area, ε, was based on the density of fish in a menhaden school.

Table 1 Input data

Laser power (p^{rad})	1 kw
Beam radius at water surface (a)	0.5 m
Grid element area (ΔA)	0.0314 m^2
Ratio of target area to grid area (ε)	0.5
Target reflectivity (R_t)	0.05
Receiver area (A_r)	0.13 m^2

The power density distribution is plotted in Fig. 5 at three depths for $v_0 = 0°$ and $v_0 = 90°$, i.e., in the direction of the wind source and perpendicular to the wind source. A wind velocity of 5.0 m/sec and a volume attenuation coefficient of 0.2 m^{-1} (clear coastal water) were used. The underwater power density curves are terminated at the distance from the beam centerline at which the received power at the airborne detector is below the "cut-off" of 10^{-8} w. Only at the outer regions of the power density curves is there any appreciable difference between $P_d(\mu_0, v_0 = 0°, z)$ and $P(\mu_0, v_0 = 90°, z)$. Because of this, and also since these outer regions have lower power density and therefore lower reflected power than regions closer to the beam centerline, the underwater power density for a given distance out from the beam centerline, for a constant μ_0 and constant depth, is taken to be the average of $P_d(\mu_0, v_0 = 0°, z)$ and $P_d(\mu_0, v_0 = 90°, z)$, i.e.,

$$P_d(\mu_0, v_0, z) = \frac{P_d(\mu_0, v_0 = 0°, z) + P_d(\mu_0, v_0 = 90°, z)}{2} \quad (43)$$

This approximation greatly reduces the amount of computer time required to determine the received power at the airborne detector and introduces no significant error.

The power received at the airborne detector is presented in Fig. 6 for three wind velocities W and two altitudes of the receiver above the ocean surface, h (for the laser radiation incident normal to the ocean surface, $h = r_1$). A volume attenuation coefficient, γ, of 0.2 m^{-1} was used in the calculation. Figure 6 is more general than it appears since it is not restricted to the altitudes of 100 ft and 500 ft nor to the laser output power level of 1 kw. The received target reflected power at any altitude h and for any laser power p^{rad} can be obtained by multiplying the power received at 100 ft for a 1 kw laser by $\{[100\,(\text{ft})/h\,(\text{ft})]^2\, p^{rad}\,(\text{kw})\}$, as can be seen by examining Eq. (39).

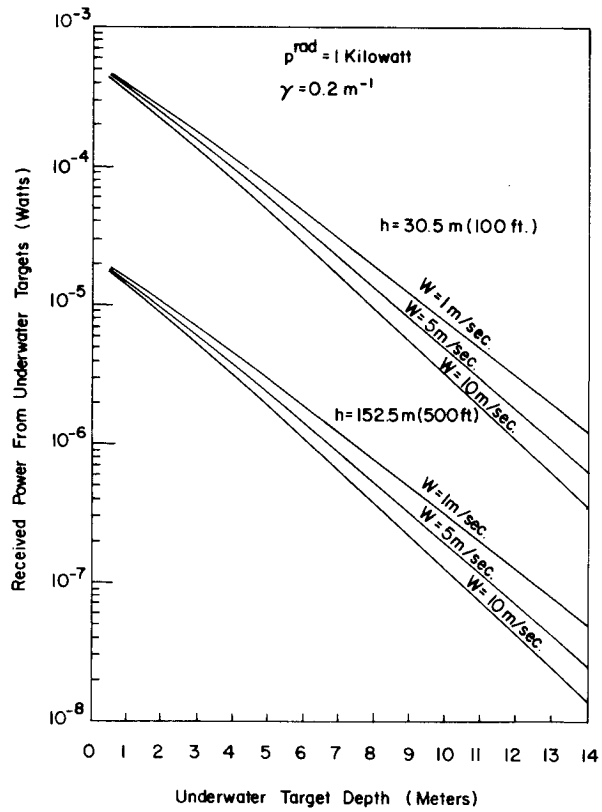

Fig. 6 Received power at airborne detector from underwater targets.

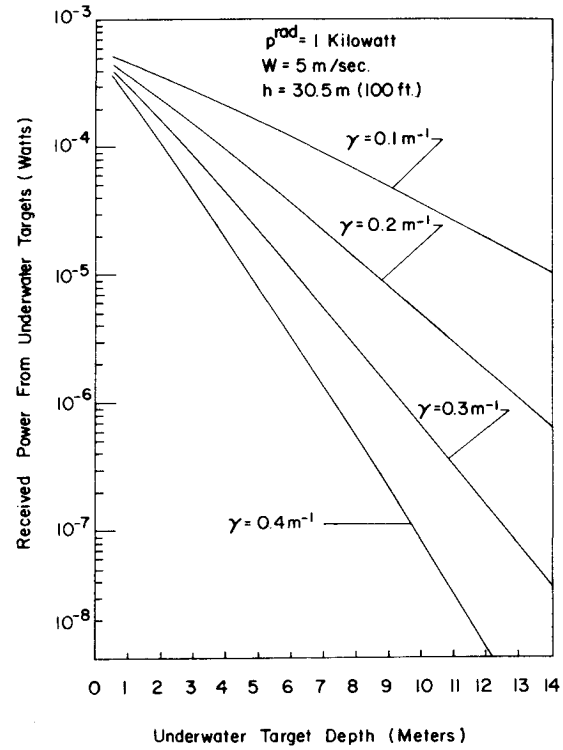

Fig. 7 Dependence of received power at airborne detector from underwater targets on volume attenuation coefficient.

As shown in Fig. 6, for a laser power level of 1 kw and the input data employed, the received power at the airborne detector is greater than the minimum detectable power level of the RCA C21117C 40 mm SIT camera tube for any altitude less than 500 ft and any wind velocity less than 10 m/sec for targets located to 10 m in depth. For a photodiode receiving system having a minimum detectable power level of 10^{-5} w, the airborne detector altitude could be higher and/or the targets located at a deeper depth. Increasing the laser output power above 1 kw would increase the received power for a given target depth or increase the depth of a detectable target for a given detector altitude.

The importance of using a laser wavelength for which a minimum value of the volume attenuation coefficient is obtained is illustrated in Fig. 7. The larger the volume attenuation coefficient, the more rapid the decrease in received power with increasing depth. For example, for a wind velocity of 5 m/sec and an aircraft altitude of 100 ft, there is a decrease of almost 3 orders of magnitude in the received power from a target at a depth of 10 m for a γ of 0.4 m^{-1} as compared to the received signal from radiation with a γ of 0.1 m^{-1}. Similar to Fig. 6, the power received by the airborne detector plotted in Fig. 7 can be scaled for any altitude and any laser power.

For obtaining maximum depths in fish location, it is therefore more important to sense the spectral characteristics of the water under examination and tune the laser to the desired wavelength than to employ a very high power laser which can operate at only a fixed wavelength. The functional dependence of the reflectivity of the particular fish under search on the laser wavelength must also be considered to determine maximum returned signal.

The underwater spreading of the laser beam due to surface refraction for three wind velocities is illustrated in Fig. 8. The region to the left of each curve is the zone which contributes to the total received power by the airborne detector, above the "cut-off" of 10^{-8} w, at 100 ft altitude. Figure 9 illustrates an airborne view of the variation of the "zone of target detectability"

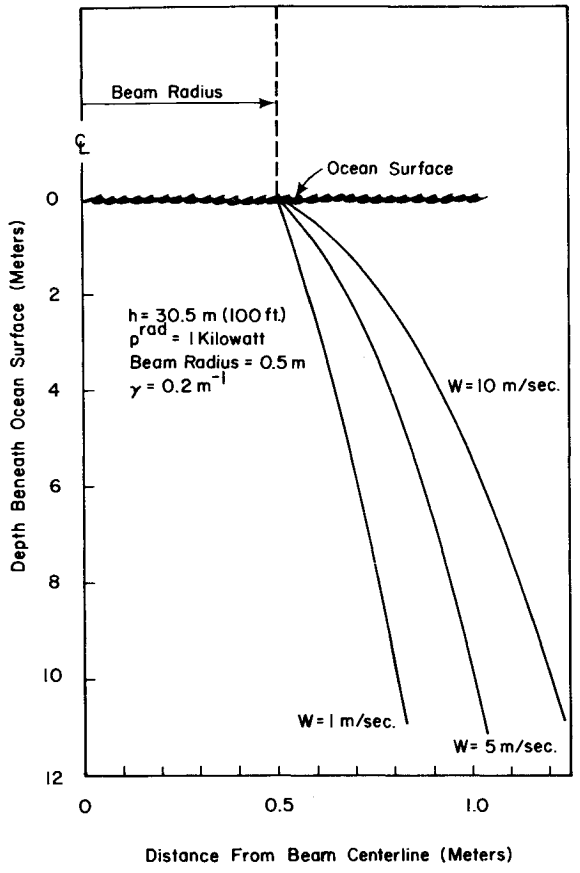

Fig. 8 Underwater beam spreading due to surface refraction.

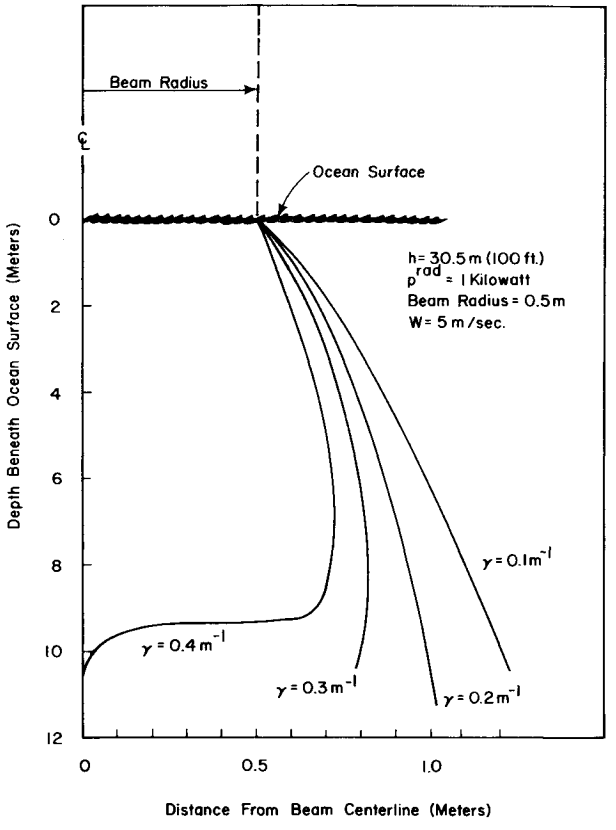

Fig. 10 Effect of volume attenuation coefficient on zone of target detectability.

with depth for a γ of 0.2 m^{-1}, a detector altitude of 100 ft, and a wind velocity of 5 m/sec. Figures 8 and 9 illustrate that fish detection, at a given depth, occurs over a greater area than the area of the ocean surface illuminated region.

The zone of target detectability increases with depth until the exponential nature of beam power attenuation significantly decreases the beam power density. For large γ, the beam power loss due to attenuation rapidly decreases the spreading of the target detectability zone and target detectability depth. Figure 10 illustrates the variation of the zone of target detectability with depth for various volume attenuation coefficients. This illustrates again the need for tuning the laser to the wavelength for minimum volume attenuation coefficient.

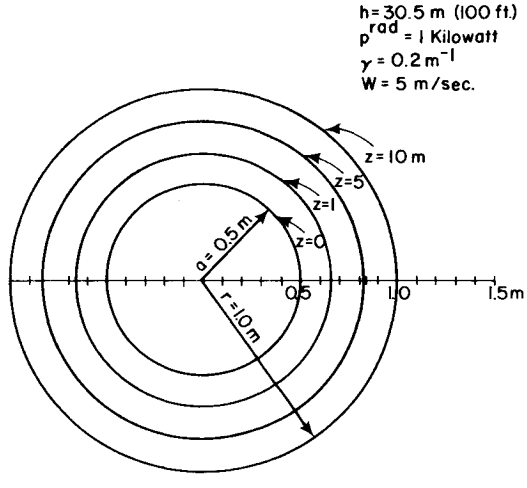

Fig. 9 Aircraft view of the zone of target detectability for various depths.

IV. System and Signal/Noise Considerations

A pulsed laser, for maximum power output, and a gated receiver with appropriate filters and spatial arrangement for preventing overloading of the photocathode of the detector, capable of near elimination of surface reflection saturation and reduction of underwater backscatter, is required. The laser must be tunable in the blue-green spectrum to optimize for minimum laser attenuation and maximum fish reflection. The gated receiver must be capable of detection of very low power levels ($\sim 10^{-7}$ w) in very short time durations ($\sim 10^{-8}$ sec).

A receiving telescope system would gather the reflected laser radiation from the underwater targets. After reception by the receiving telescope, the radiation would be filtered by an optical spectrum analyzer, narrow-band filters, and spatial filters.[6] All naturally occurring radiation and fluorescence would be filtered out which does not occur at the laser wavelength being transmitted by the interferometer and filter system. Any transmitted visible light fluorescence and transpectral effects would be too minute to contribute significantly to signal noise.[6] The transmitted light would then be detected with a photodiode or photomultiplier, with the detected signal displayed on an oscilloscope or chart recorder.

Ultra-sensitive avalanche photodiode detection modules with a noise equivalent power (NEP) of 5×10^{-9} w are presently state-of-the-art. Employing a receiving telescope with an 8-in. aperture, the minimum detectable power density at the airborne receiver is 1.5×10^{-7} w/m^2 for such a photodiode system. Gated photomultipliers and diodes are very sensitive and provide an output that is ideal for the time delay measurements required. They will also provide slant range to the target when used in conjunction with an oscilloscope ("A" scope) or a "Beta scan" display. With an "A" scope the time delay between laser pulse initiation and reception is a direct measure of the slant range to the target. With a "Beta scan" the targets appear in slant range but there is also an indication as to their angle off the perpendicular to the axis of the aircraft.

An estimate of the total laser power backscattered due to volumetric scattering[7] from a grid element ΔA located at (μ_0, v_0, z) with differential thickness dz is

$$d(\Delta p_b) = \Delta A P_0 2\pi \int_{\pi/2}^{\pi} e^{-\gamma z} \sigma(\theta) \sin\theta \, d\theta \, dz \tag{44}$$

where $\sigma(\theta)$ is the volume scattering function and is related to the total volume scattering function s by

$$s = 2\pi \int_0^{\pi} \sigma(\theta) \sin\theta \, d\theta \tag{45}$$

Equation (44) does not take into account the laser beam dispersion caused by the distribution of refracting elementary water surface facets, and therefore will result in an over estimation of the backscattered power that will be received at the airborne detector. This follows since the refracting elementary surface facets reduce the power density at each grid element ΔA beneath the illuminated surface region below the value of a nonrefracted beam (Fig. 5). Also, since the underwater power density is much less at grid elements outside of the illuminated surface region than for grid elements beneath the illuminated surface region, the major grid contributors to detector received backscatter are those beneath the illuminated surface region.

In general, the volumetric scattering is predominantly in the forward direction, characterized by $\sigma(\theta)$ being sharply peaked about $\theta = 0$, with $\sigma(\theta)$ approximately constant in the back direction, $\pi/2 \leqq \theta \leqq \pi$. Thus we may consider[7]

$$\sigma(\theta) \simeq b/2\pi, \qquad \pi/2 \leqq \theta \leqq \pi \tag{46}$$

where b is the backscatter coefficient defined as

$$b = 2\pi \int_{\pi/2}^{\pi} \sigma(\theta) \sin\theta \, d\theta \tag{47}$$

Measurements of the backscatter coefficient have been made by Tyler.[8] For certain Pacific Coastal and offshore water Tyler obtained that b ranged from 0.0063 m^{-1} to 0.000847 m^{-1}. In these measurements Tyler used signals that were bandwidth limited by a Wratten No. 57 filter (peak transmittance at about 522 nm with a halfband width of about 80 nm). Since the scattering of light in the ocean is predominantly due to transparent biological organisms and particles large compared with the wavelength of light, the magnitude of scattering is virtually independent of wavelength.[6]

Substitution of Eq. (46) into Eq. (44) yields

$$d(\Delta p_b) = \Delta A b P_0 e^{-\gamma z} dz \tag{48}$$

The total volumetric backscattered power from a grid element ΔA located at (μ_0, v_0, z) with thickness Δz is obtained by integrating Eq. (48) between the limits z and $z + \Delta z$, yielding

$$\Delta p_b = \Delta A b P_0 \frac{e^{-\gamma z} - e^{-\gamma(z+\Delta z)}}{\gamma} \tag{49}$$

Now $P_0 e^{-\gamma z}$ can be approximated by $P_d(\mu_0, v_0, z)$, retaining the overestimation of Δp_b beneath the illuminated surface region. Further assurance of an overestimation of the volumetric backscatter is that the total volume element $\Delta A \Delta z$ is considered to contribute to the backscatter with *no reduction due to fish being in this zone*. Therefore

$$\Delta p_b = \Delta A b P_d(\mu_0, v_0, z) \frac{(1 - e^{-\gamma \Delta z})}{\gamma} \tag{50}$$

For the gated receiver, the volumetric thickness Δz is determined by the receiver gate time.

The power reflected from the targets located at (μ_0, v_0, z) is given by Eq. (24). Thus with Eqs. (24) and (50), we have an estimate of the signal reflected power to the noise reflected power. Under the stated approximations, Eqs. (24) and (50) are valid for all the grid elements at a given depth. Consequently, an underestimation of the S/N for volumetric backscattering at a given depth z and slab thickness Δz, is

$$\mathrm{S/N} = \varepsilon R_t (\gamma/b)/(1 - e^{-\gamma \Delta z}) \tag{51}$$

For Eq. (51) the targets have been assumed to be near the top of the volumetric backscattered region of thickness Δz, which can be experimentally achieved by proper receiver gating.

Tyler experimentally measured values of γ/b ranging from 112.8 for near-shore waters to 152.3 for offshore waters.[8] An estimate of the worst case of S/N can be obtained by considering Δz to be sufficiently large so that $1 - e^{-\gamma \Delta z} \approx 1$. Using the values of ε and R_t given in Table 1, the worst-case estimate of S/N is

$$3 \leqq \mathrm{S/N} \lesssim 4 \tag{52}$$

It is within the state-of-the-art to gate the receiver so that Δz can be on the order of 3 m.[9] Backscatter from depths above and below this 3 m slab is gated out. For a 3 m gated underwater slab, the underestimated S/N range is

$$3.5 \leqq \mathrm{S/N} \lesssim 12 \tag{53}$$

A higher fish density and higher fish reflectance than used in the previous calculations will yield a higher S/N. Since the spectral reflectance of fish is wavelength dependent,[10] proper tuning of the laser to increase R_t from 0.05 to 0.10 would increase S/N from 12 to 24. For cases when fish turn on their sides or in a belly-up position during schooling, such that the silvery underside increases the reflectance, S/N will likewise increase.

In addition to the filtering of naturally occurring radiation and the gating and filtering technique to eliminate surface reflection and reduce volumetric underwater backscattering, circular polarization techniques[11,12] can also be employed to further reduce underwater backscatter and increase S/N above the minimum values given above. With further advances in transmitted laser power, the ratio of received signal to detector shot noise will also increase.[7]

V. Conclusion

The results from the developed mathematical model, using input parameters of presently available equipment and estimates of fish school density and reflectivity, reveal that the power received at an airborne detector from fish reflected incident laser radiation and the S/N are of sufficient magnitude to locate fish schools with an airborne remote sensing laser system.

References

[1] Swennen, J. P. J. W., "Time-Average Power-Density Probability Distribution Below the Ocean Surface of a Beam of Collimated Optical Radiation Incident on the Surface," *Journal of the Optical Society of America*, Vol. 56, No. 2, Feb. 1966, pp. 224–229.

[2] Cox, C. and Munk, W., "Slopes of the Sea Surface Deduced From Photographs of Sun Glitter," Bulletin, Scripps Institution of Oceanography, Univ. of Calif., San Diego, Calif., Vol. 6, 1956, pp. 401–487.

[3] Born, M. and Wolf, E., *Principles of Optics*, 3rd ed., Pergamon Press, New York, 1965, pp. 41–47.

[4] Collin, R. E., "The Receiving Antenna," in *Antenna Theory: Part 1*, edited by R. E. Collin and F. J. Zucker, McGraw-Hill, New York, 1969, pp. 94–98.

[5] Swarner, W. G., "An Optical Spatial Filter for Achieving Wide Dynamic Range in Air-to-Water Optical Transmission," *Applied Optics*, Vol. 9, No. 2, Feb. 1970, pp. 507–509.

[6] Duntley, S. Q., "Light in the Sea," *Journal of the Optical Society of America*, Vol. 53, No. 2, Feb. 1963, pp. 214–233.

[7] Hodara, H. and Marquedant, R. J., "The Signal/Noise Ratio Concept in Underwater Optics," *Applied Optics*, Vol. 7, No. 3, March 1968, pp. 527–534.

[8] Tyler, J. A., "Scattering Properties of Distilled and Natural Waters," *Limnology and Oceanography*, Vol. 6, No. 1, Jan. 1961, pp. 451–456.

[9] Kadrmas, K. A., "Phased-Array Laser Radar: Concept and Application," TM X-64753, June 8, 1973, NASA.

[10] Project Staff, "Final Report, Fish Identification by Remote Sensing," Rept. 11435-6001-RO-00, Dec. 23, 1968, TRW Systems Group, Redondo Beach, Calif.

[11] Gilbert, G. D. and Pernicka, J. C., "Improvement of Underwater Visibility by Reduction of Backscatter with a Circular Polarization Technique," *Applied Optics*, Vol. 6, No. 4, April 1967, pp. 741–746.

[12] Gilbert, G. D., "The Effects of Particle Size on Contrast Improvement of Polarization Discrimination for Underwater Targets," *Applied Optics*, Vol. 9, No. 2, Feb. 1970, pp. 421–428.